An efficient method for computing hyperbolic systems with geometrical source terms having concentrations*

Shi Jin † and Xin Wen ‡

Dedicated to Professor Zhong-ci Shi on the occasion of his seventieth birthday

Abstract

We propose a simple numerical method for calculating both unsteady and steady state solution of hyperbolic system with geometrical source terms having concentrations. Physical problems under consideration include the shallow water equations with topography, and the quasi one-dimensional nozzle flows. We use the interface value, rather than the cell-averages, for the source terms, which results in a well-balanced scheme that can capture the steady state solution with a remarkable accuracy. This method approximates the source terms via the numerical fluxes produced by an (approximate) Riemann solver for the homogeneous hyperbolic systems with slight additional computation complexity using Newton's iterations and numerical integrations. This method solves well the sub- or super-critical flows, and with a transonic fix, also handles well the transonic flows over the concentration. Numerical examples provide strong evidence on the effectiveness of this new method for both unsteady and steady state calculations.

*Research supported in part by U.S. National Science Foundation grant No. DMS-0305080, National Natural Science Foundation of China Project 10228101 and the Basic Research Projects of Tsinghua University under the Project JC2002010.

†Department of Mathematical Sciences, Tsinghua University, Beijing 100084, P.R. China, and Department of Mathematics, University of Wisconsin, Madison, WI 53706, USA. Email address: jin@math.wisc.edu.

‡Department of Mathematical Science, Tsinghua University, Beijing 100084, P.R. China. Email address: wenx@mail.tsinghua.edu.cn.

1 Introduction

Hyperbolic systems with geometric source terms arise in many physical applications, including the shallow water equations with bottom topography and the quasi one-dimensional nozzle flow equations with variable cross-sectional area. When the source terms in the system have concentrations, corresponding to a δ function in the source, the usual numerical method for source term approximation may give poor approximations to the steady state equations due to the first order numerical viscosity used at discontinuities [12]. A well accepted strategy for such problems is to design so called *well-balanced* scheme that balances the numerical flux with the source term such that the steady state solution is captured numerical with exactly or with at least a second order accuracy. Many well-balanced schemes have been proposed by many authors in recent years, including well-balanced scheme based on non-conservative product [12] and its extensions [13], [11], [5], [6], [9], [10], LeVeque's quasi-steady scheme [18], kinetic schemes [4], [19], [2], [25], relaxation schemes [20], central schemes [15]. Nonlinear extension of Roe's linear idea [23] was made in [3], [24], [14]. Most of these methods require the modification of the numerical flux.

The interface method of Jin [14] uses the numerical flux for the homogeneous hyperbolic systems in the source term, and was shown in [14] that for smooth solutions, it captures the steady state at *cell interfaces* with a second order accuracy, thus is well-balanced. Designed for Godunov [8] and Roe [22] type schemes, this method has the advantage that it does not require any modification of the numerical flux for the convection term. By using the numerical flux directly in the source term it needs almost no additional computation complexity to deal with source term.

In this paper we derive a new set of well-balanced scheme that can be viewed as an improvement of Jin's interface method. It is a hybridization of the conventional cell average method with a improved interface type method at concentration points. The main idea is based on finite volume approximation of hyperbolic systems, with a more accurate approximation of the volume average of the source term. While Jin's interface method can be viewed as the trapezoidal approximation of this source average, we found that more accurate approximation of the source average significantly improves the approximation of the steady state solutions. This involves more accurate numerical integrations and Newton's iterations, but the added computational compexity, compared to the interface method, is small. This new method can accurately capture both unsteady and steady state solutions. Moreover, with a simply fix, it is capable of handling the transonic flows at source concentrations.

In section 2, 3 and 4 we introduce our method for the shallow water equations, isothermal and non-isothermal nozzle flow equations respectively. The property of preservation of steady state equations is shown. Numerical examples show that the new method gives satisfactory unsteady and steady state solutions.

In the sequel we will use $x_{j+1/2}$ to denote the grid point, $\Delta x = x_{j+1/2} - x_{j-1/2}$ the mesh size, $w_{j+1/2} = w(x_{j+1/2})$ the interface value of a general quantity w, and $w_j = \frac{1}{\Delta x}\int_{x_{j-1/2}}^{x_{j+1/2}} w(x)\,dx$ be the cell average of w over the cell $[x_{j-1/2}, x_{j+1/2}]$.

2 The shallow water equations

Consider the one-dimensional shallow water equations with topography

$$h_t + (hv)_x = 0, \tag{2.1}$$

$$(hv)_t + (hv^2 + \frac{1}{2}gh^2)_x = -ghB_x\,, \tag{2.2}$$

where h is the depth of the water, u is the mean velocity, g is the gravitational constant, and $B(x)$ is the bottom topograph. The steady state solutions satisfy

$$hv = C_1, \tag{2.3}$$

$$\frac{1}{2}v^2 + gh + gB = C_2. \tag{2.4}$$

These steady state conditions are satisfied not only on smooth part of the solution, but also across a bottom discontinuity [1]. A numerical method is called *well-balanced* [12] if it satisfies the steady state conditions (2.3), (2.4) exactly or with at least second order accuracy even when the bottom contains discontinuities. In this section we design a well-balanced scheme for (2.1), (2.2) which can preserve these steady states even at cells containing discontinuity of $B(x)$.

2.1 A hybrid method

We first present the conventional *cell average method*,

$$\partial_t h_j + \frac{(hv)_{j+\frac{1}{2}} - (hv)_{j-\frac{1}{2}}}{\Delta x} = 0, \tag{2.5}$$

$$\begin{aligned} &\partial_t (hv)_j + \frac{(hv^2 + \frac{1}{2}gh^2)_{j+\frac{1}{2}} - (hv^2 + \frac{1}{2}gh^2)_{j-\frac{1}{2}}}{\Delta x} \\ = \;& -gh_j \frac{B_{j+\frac{1}{2}} - B_{j-\frac{1}{2}}}{\Delta x}. \end{aligned} \tag{2.6}$$

where $B_{j+\frac{1}{2}} = B(x_{j+\frac{1}{2}})$, and the numerical flux is a Godunov [8] or Roe [22] flux or its higher order extensions.

As is well known, the cell average method is suitable if the bottom function $B(x)$ is continuous. When $B(x)$ contains a discontinuity, the cell average method generally fails to be well-balanced due to the first order numerical viscosity added at discontinuities. This matches with the fact that the shallow water equations in the form (2.1), (2.2), which are referred to as mass-momentum formulation in [1], no longer hold valid when the bottom slope becomes infinite.

We also mention the interface method of Jin [14]:

$$\partial_t h_j + \frac{(hv)_{j+\frac{1}{2}} - (hv)_{j-\frac{1}{2}}}{\Delta x} = 0, \tag{2.7}$$

$$\partial_t(hv)_j + \frac{(hv^2+\frac{1}{2}gh^2)_{j+\frac{1}{2}} - (hv^2+\frac{1}{2}gh^2)_{j-\frac{1}{2}}}{\Delta x}$$
$$= -g\frac{h_{j+\frac{1}{2}}+h_{j-\frac{1}{2}}}{2}\frac{B_{j+\frac{1}{2}}-B_{j-\frac{1}{2}}}{\Delta x}. \tag{2.8}$$

As will be shown later, the new method developed in this paper is a generalization– with a better accuracy to preserve the steady state solution– of this method.

Our new method is a hybrid of the cell average method in cells in which $B(x)$ is continuous with a modification of the source term approximation in cells which contain a discontinuity of $B(x)$.

Assume a discontinuity of $B(x)$ is contained in the middle of a cell $[x_1, x_2]$. Usually we use $[x_{j-\frac{1}{2}}, x_{j+\frac{1}{2}}]$ to denote a cell. Here we use the subindex 1, 2 in order to simplify the notation. Denote $\widetilde{h}, \widetilde{m}$ to be averages of h, hv in this cell respectively, and $h_1, h_2, v_1, v_2, B_1, B_2$ to be the interface values of h, v, B at x_1, x_2 respectively.

Our hybrid scheme in the cell $[x_1, x_2]$ takes the form

$$\widetilde{h}_t + \frac{(h_2v_2)-(h_1v_1)}{\Delta x} = 0, \tag{2.9}$$
$$\widetilde{m}_t + \frac{(h_2v_2^2+\frac{1}{2}gh_2^2)-(h_1v_1^2+\frac{1}{2}gh_1^2)}{\Delta x}$$
$$= -\frac{g}{\Delta x}\int_{x_1}^{x_2}\widehat{h}\widehat{B}_x dx; \tag{2.10}$$

where a general hat-function $\widehat{q}$ denotes a *smooth function* in cell $[x_1, x_2]$ with end-point values $q(x_i)$ at $x_i (i = 1, 2)$. The choice of the non-negative smooth function $\widehat{h}$ over $[x_1, x_2]$ will be made clear later.

Now define function $H(x)$ in cell $[x_1, x_2]$ to be the *linear interpolant* through interpolating points $(x_i, h_iv_i), i = 1, 2$, and $G(x)$ in $[x_1, x_2]$ to be the linear interpolant through $(x_i, \frac{1}{2}v_i^2 + gh_i + gB_i), i = 1, 2$. Namely,

$$H(x_i) = h_iv_i, \quad G(x_i) = \frac{1}{2}v_i^2 + gh_i + gB_i, \qquad i = 1, 2. \tag{2.11}$$

We then determine $\widehat{h}, \widehat{v}$ from the identities

$$H = \widehat{h}\widehat{v}, \tag{2.12}$$
$$G = \frac{1}{2}\widehat{v}^2 + g\widehat{h} + g\widehat{B}, \tag{2.13}$$

or $\widehat{h}$ can be determined by the relation

$$\frac{1}{2}\frac{H^2}{\widehat{h}^2} + g\widehat{h} + g\widehat{B} = G. \tag{2.14}$$

We now prove that our hybrid scheme is well-balanced. We just need to prove this property across the cell $[x_1, x_2]$ that contains a discontinuity of $B(x)$.

Theorem 2.1. *Our hybrid scheme can preserve the steady state conditions (2.3)-(2.4) exactly at cell interfaces at two sides of bottom discontinuity:*

$$h_1 v_1 = h_2 v_2, \tag{2.15}$$

$$\frac{1}{2}v_1^2 + gh_1 + gB_1 = \frac{1}{2}v_2^2 + gh_2 + gB_2. \tag{2.16}$$

Proof. It is directly seen from (2.9) that when steady state is reached, the numerical solution should give $h_1 v_1 = h_2 v_2$, thus condition (2.15) is satisfied. It remains to prove condition (2.16) holds in the steady state solution. This is equivalent to prove that $G(x_1) = G(x_2)$.

Let E_2, defined in cell $[x_1, x_2]$, be given by

$$E_2 = (\widehat{h}\widehat{v}^2)_x + (\frac{1}{2}g\widehat{h}^2)_x + g\widehat{h}\widehat{B}_x. \tag{2.17}$$

One can transfer the expression (2.10) into the form

$$\widetilde{m}_t = -\frac{1}{\Delta x}\int_{x_1}^{x_2} E_2 dx\,. \tag{2.18}$$

Since all the hat-functions are smooth, one has

$$\begin{aligned} E_2 &= (\widehat{h}\widehat{v})_x\widehat{v} + (\widehat{h}\widehat{v})\widehat{v}_x + g\widehat{h}\widehat{h}_x + g\widehat{h}\widehat{B}_x \\ &= H_x\widehat{v} + \widehat{h}(\widehat{v}\widehat{v}_x + g\widehat{h}_x + g\widehat{B}_x) \\ &= H_x\widehat{v} + \widehat{h}G_x, \end{aligned} \tag{2.19}$$

by recalling the definition of H, G in (2.12), (2.13).

Since H is linear in $[x_1, x_2]$, with the proved condition (2.15), we know that, at steady state, H is a constant, and hence H_x must be zero in the cell $[x_1, x_2]$. So in the cell $[x_1, x_2]$

$$E_2 = \widehat{h}G_x. \tag{2.20}$$

On the other hand, from (2.18) we know that the steady state solution satisfies

$$\int_{x_1}^{x_2} E_2 dx = 0\,,$$

thus

$$\int_{x_1}^{x_2} \widehat{h}G_x dx = 0. \tag{2.21}$$

Since G is linear in $[x_1, x_2]$, thus G_x is a constant. If $h_1 = 0, h_2 = 0$ at steady state solution, then (2.21) holds since $\hat{h} = 0$. This is a vacuum state. If at least one

of h_1, h_2 is greater than zero, since $\widehat{h}(x)$ is chosen to be non-negative and smooth in $[x_1, x_2]$, the integration of $\widehat{h}(x)$ in $[x_1, x_2]$ is positive. Thus equality (2.21) forces $G_x = 0$ in $[x_1, x_2]$, and consequently $G(x_1) = G(x_2)$ at steady state.

□

In practical calculation, we need to solve $\widehat{h}$ from H, G using (2.14). We fix the choice of $\widehat{B}$ as a linear function in $[x_1, x_2]$ with $\widehat{B}(x_1) = B_1, \widehat{B}(x_2) = B_2$. Then the source term approximation on the right hand side of our hybrid scheme (2.10) turns out to be

$$-g\left(\frac{1}{\Delta x}\int_{x_1}^{x_2}\widehat{h}dx\right)\frac{B_2 - B_1}{\Delta x}. \tag{2.22}$$

Thus in computation we need to obtain the cell average of $\widehat{h}$ on $[x_1, x_2]$

$$\frac{1}{\Delta x}\int_{x_1}^{x_2}\widehat{h}dx$$

to get the source term approximation (2.22). Notice if we use the trapezoidal rule on the whole interval $[x_1, x_2]$, then we recover the interface method of Jin given in (2.7)-(2.8). Since $\widehat{h}$ has a large gradient over $[x_1, x_2]$, this is not a very accurate approximation. One of the main strategy of the new method is to approximate the above integration *more accurately*. In our computation we divide the interval $[x_1, x_2]$ into five subintervals and use Simpson's rule on each subinterval to perform the numerical integration. In practice this implementation is accurate enough in that the error between integration value we obtained and the "exact" value, which is obtained by using much more subintervals to compute the integration, is small enough. The needed values of $\widehat{h}$ to perform the numerical integration are obtained by using Newton iteration to solve the equation (2.14). These Newton iterations can be executed consecutively, and one can use the solution of previous one to be the initial value, thus each Newton iteration converges with very few iterations.

2.2 A transonic fix

For fixed values of $\widehat{B}, H, G$, equation (2.14) generally has two solutions for $\widehat{h}$, one corresponding to the subcritical state and another to the supercritical state. When the problem is in the subcritical case, $|\frac{v_1}{\sqrt{gh_1}}| < 1$ and $|\frac{v_2}{\sqrt{gh_2}}| < 1$, we choose $\widehat{h}$ to be the solution of (2.14) corresponding to subcritical state. On the other hand, when the problem is in the supercritical case, $|\frac{v_1}{\sqrt{gh_1}}| > 1$ and $|\frac{v_2}{\sqrt{gh_2}}| > 1$, we choose $\widehat{h}$ corresponding to the supercritical state. So there is no confusion for choosing $\widehat{h}$ from equation (2.14) in the sub- or super-critical case.

In the transonic case, we need a fix to select the correct value of $\widehat{h}$. As pointed out in [1], in a Riemann problem for the shallow water equations, when it is the transonic case, the analytic solution should reach the critical state at the higher side of the bottom jump. We can build this property into our scheme. For example, assume $|\frac{v_1}{\sqrt{gh_1}}| > 1$, $|\frac{v_2}{\sqrt{gh_2}}| < 1$, and $B_1 < B_2$. Let $H_2 = h_2 v_2$, and h_3, v_3 satisfy $h_3 v_3 = H_2$ and $|v_3| = \sqrt{gh_3}$. Namely, $h_3 = (\frac{H_2^2}{g})^{\frac{1}{3}}$ and $v_3 = \frac{H_2}{h_3}$. Denote $G_2 = \frac{1}{2}v_3^2 + gh_3 + gB_2, H_1 = H_2, G_1 = G_2$. We then can proceed to define H, G on $[x_1, x_2]$ as before (which are now constants) and find $\widehat{h}, \widehat{v}$ using (2.12)-(2.14). Clearly, by choosing $\widehat{h}$ to be solution of equation (2.14) corresponding to supercritical state, because $|\frac{v_1}{\sqrt{gh_1}}| > 1$, we obtain the solution in supercritical state at the left side of the bottom jump. We can similarly deal with other transonic case.

2.3 Numerical examples

In this subsection we give numerical examples to demonstrate that our method works well for calculating both unsteady and steady state solutions for the shallow water equations.

The following two problems are Riemann problems from [1]. The gravitational constant is set to be 9.8. These two Reimann problems are defined on the domain [-10, 10]. We use the second order shock capruting scheme based on the Roe solver with a slope limit [17], and the second order Runge-Kutta for time discretization for both problems. The zeroth order extrapolation is used as numerical boundary condition. We also obtain the "exact" solution using the new method with 1000 grid points.

Example 2.1 A Riemann problem with solution in the supercritical state

The initial data are given by $(h, v, B) = (4, -10, 0)$ when $x < 0$ and $(h, v, B) = (1, -6, 1)$ when $x > 0$. This is a supercritical case. The energy $\frac{1}{2}v^2 + h + B$ is a constant across the bottom discontinuity. We take $\frac{\Delta t}{\Delta x} = 1/20$. We compute the solution using our new method, and compare it with the solutions by the interface method and the cell average method, all using 100 cells. The results are plotted in Figures 2.1-2.3. The solutions by the new method match with the exact solution, while the solution by the cell average method severely deviates from the exact solution. Although the results from interface method look very like the result from the new method, it can not approximate the constant energy across the bottom jump as accurately as the new method. This can be seen in Figure 2.4, which is an enlargement of part of Figure 2.3. The result from the interface method allows a gap in energy across the bottom jump, which does not decrease with increased number of grid points. The energy in the steady state solution by the new method is plotted in Figure 2.5. One can see that the energy reaches a constant with a remarkable

accuracy.

Example 2.2 A Riemann problem with solution in the transonic state

The initial data are $(h, v, B) = (4, -10, 0)$ when $x < 0$ and $(h, v, B) = (2, 0, 1)$ when $x > 0$. This is a transonic case. The solution reaches the critical state at the right side of the bottom jump, and the energy $\frac{1}{2}v^2 + h + B$ remains a constant across the bottom discontinuity. We take $\frac{\Delta t}{\Delta x} = 1/50$. The solutions obtained by our new method, the interface method and the cell average method using 100 cells, along with the "exact" solution, are plotted in Figures 2.6-2.8. The solutions by the new method match very well with the real solution plotted in [1]. In particular, it can correctly predict that the Froude number reaches -1 at the right side of the bottom jump. This is due to the fix used in our method for the transonic case. On the other hand, the interface method and cell average method both fail to correctly resolve the Froude number near the bottom jump.

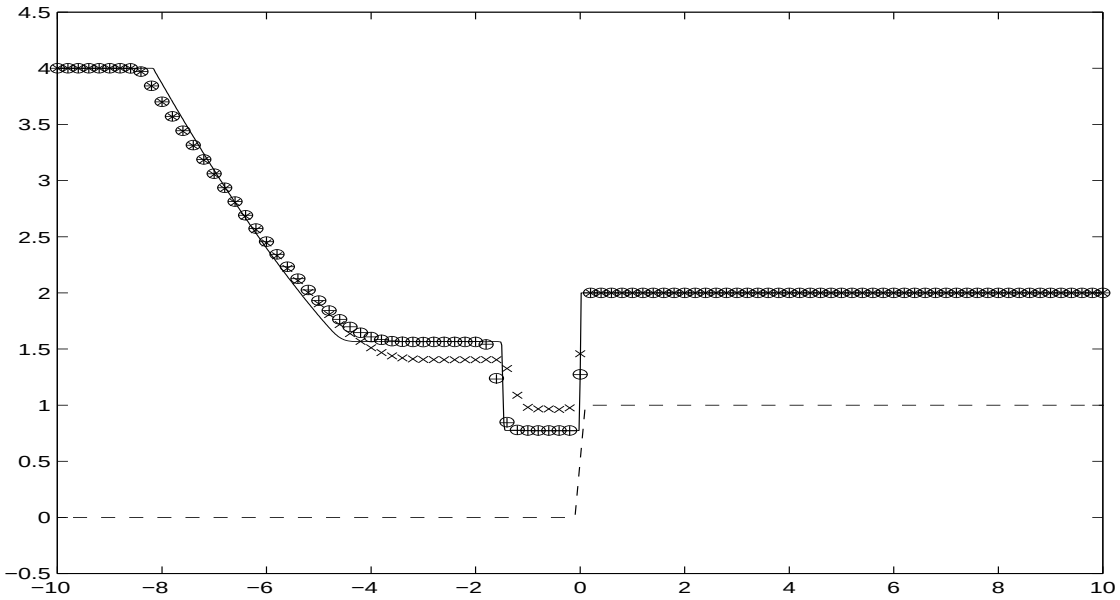

Figure 2.1 Example 2.1, the supercritical case. Water level at t=0.5 along with the bottom topography. Solid line: the exact solution; "o": the solution of our new method, "+": the solution of the interface method; "x": the solution of the cell average method; dashed line: bottom topography.

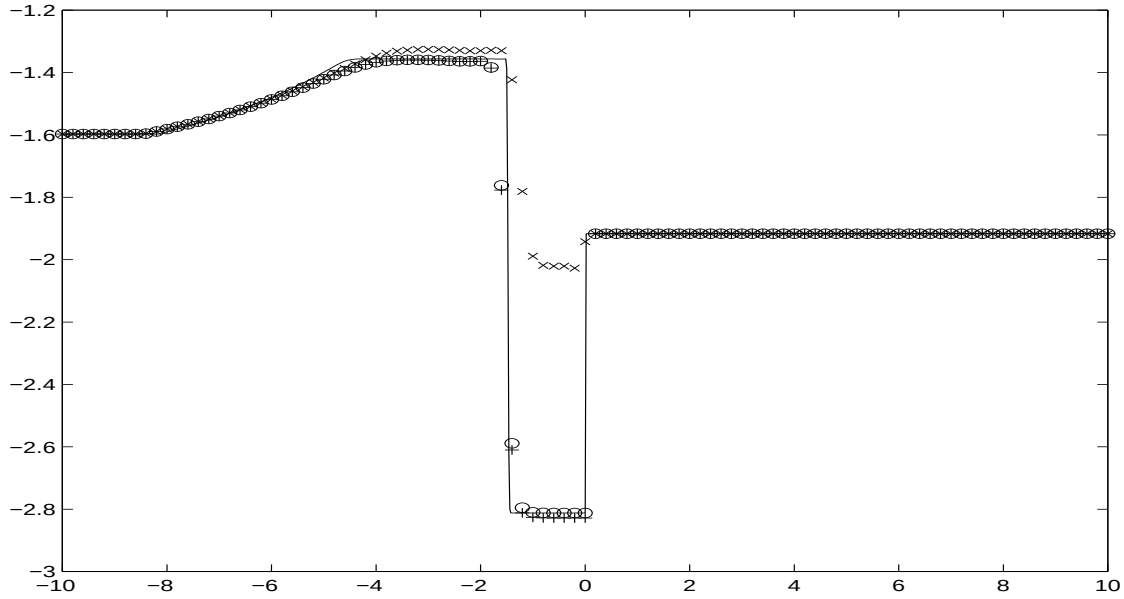

Figure 2.2 Example 2.1, supercritical case. Froude number at t=0.5. Solid line: the exact solution; "o": the solution of the new method; "+": the solution of the interface method; "x": the solution of the cell average method.

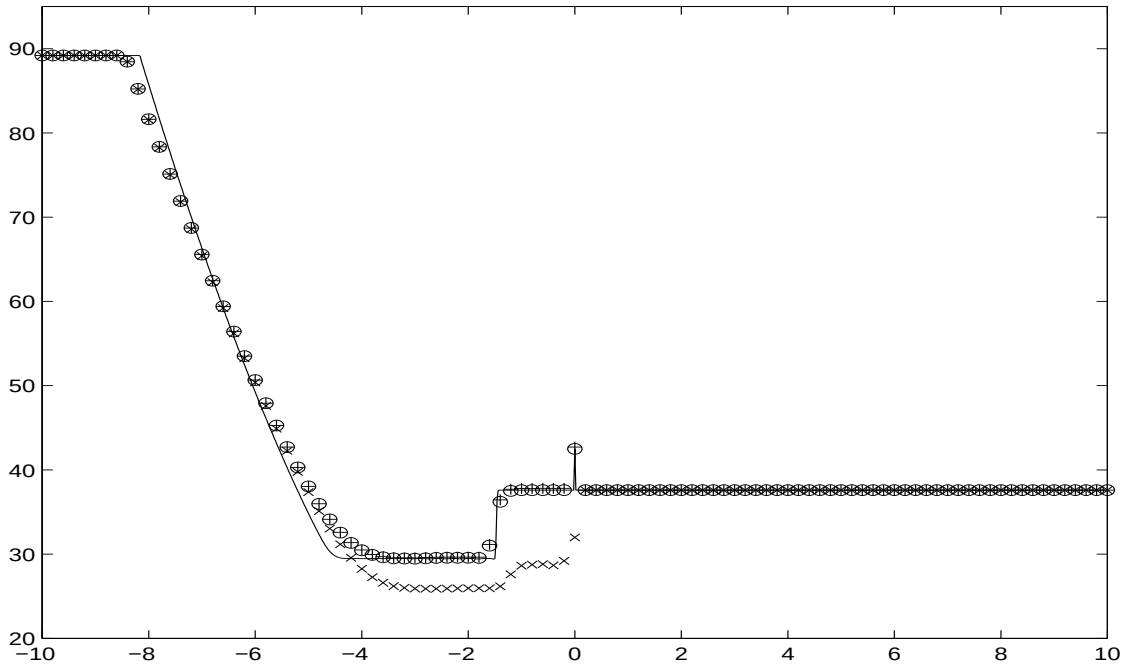

Figure 2.3 Example 2.1, supercritical case. Energy at t=0.5. Solid line: the exact solution; "o": the solution by the new method; "+": the solution of the interface method; "x": the solution of the cell average method.

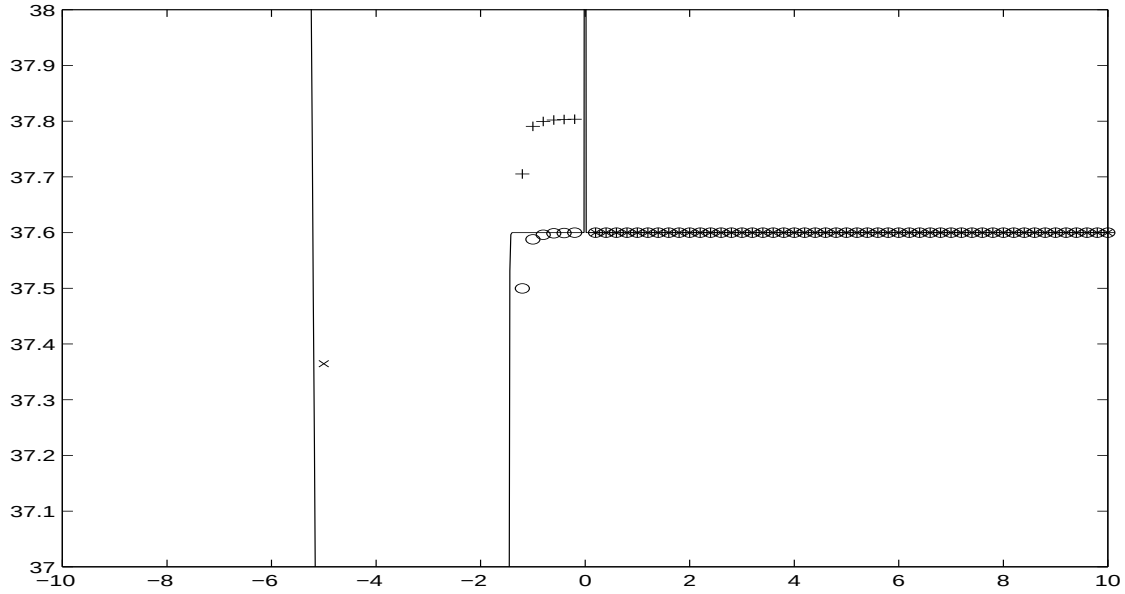

Figure 2.4 Example 2.1, supercritical case. A close look of Figure 2.3. Solid line: the exact solution; "o": the solution by the new method; "+": the solution of the interface method; "x": the solution of the cell average method.

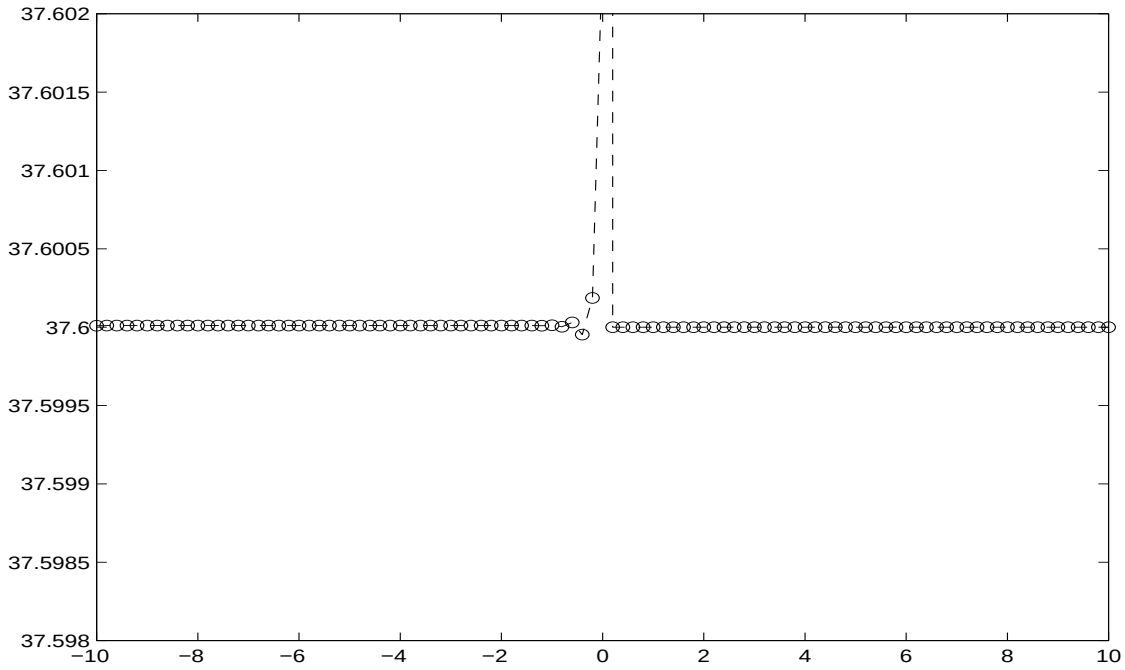

Figure 2.5 Example 2.1, the supercritical case. Steady state energy by the method using 100 cells.

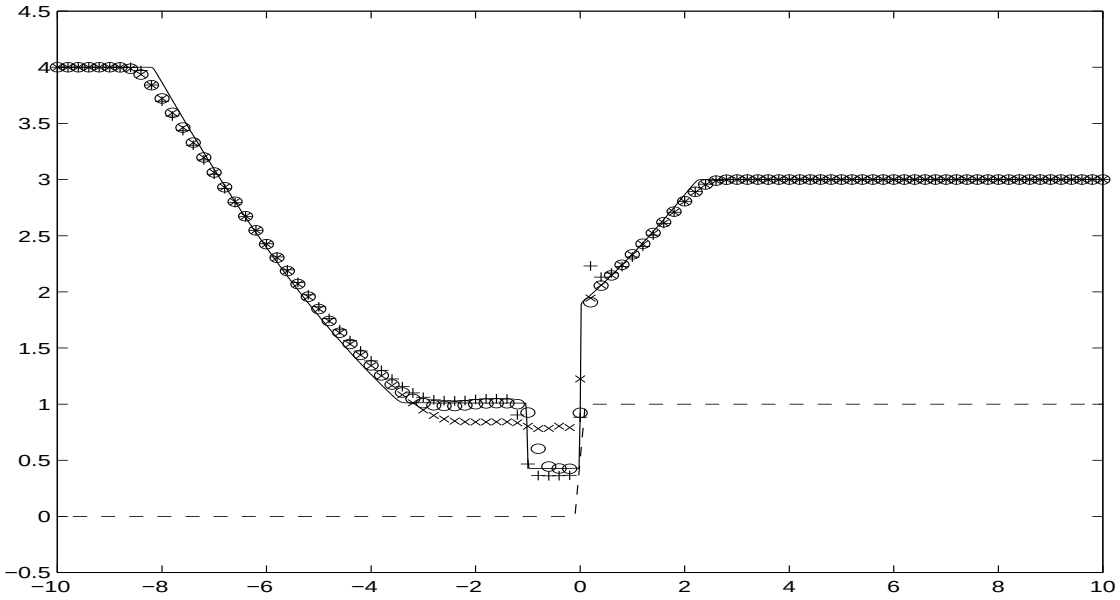

Figure 2.6 Example 2.2, the transonic case. Water level at t=0.5 along with the bottom topography. Solid line: the exact solution; "o": the solution by the new method; "+": the solution of the interface method; "x": the solution of the cell average method; dashed line: bottom topography.

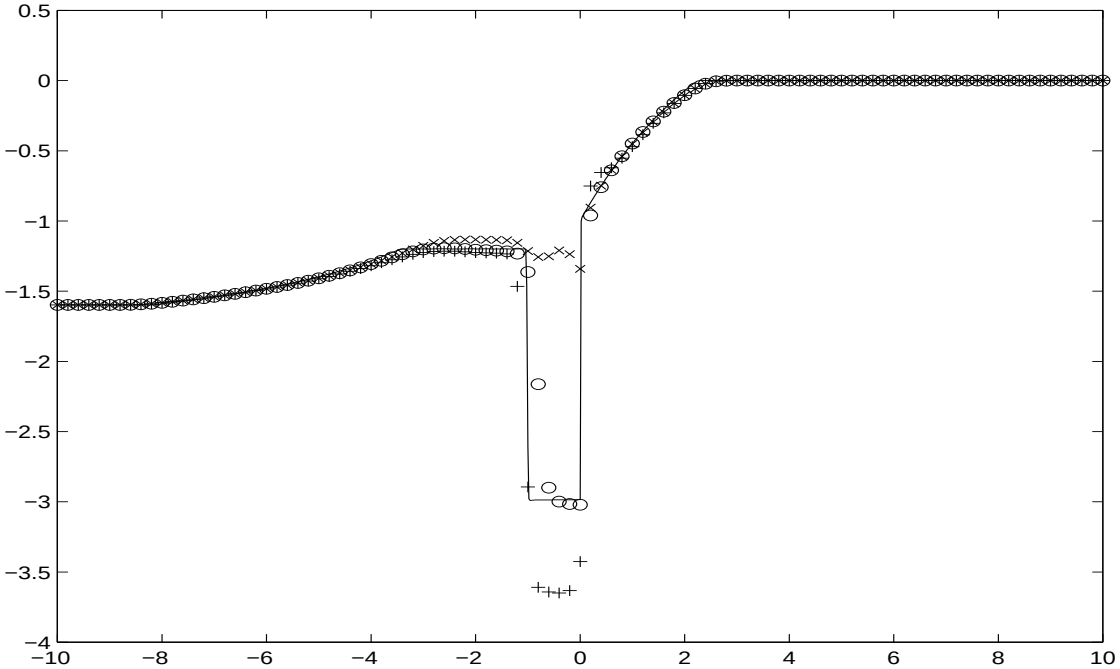

Figure 2.7 Example 2.2, the transonic case. Froude number at t=0.5. Solid line: the exact solution; "o": the solution by the new method; "+": the solution of the interface method; "x": the solution of the cell average method.

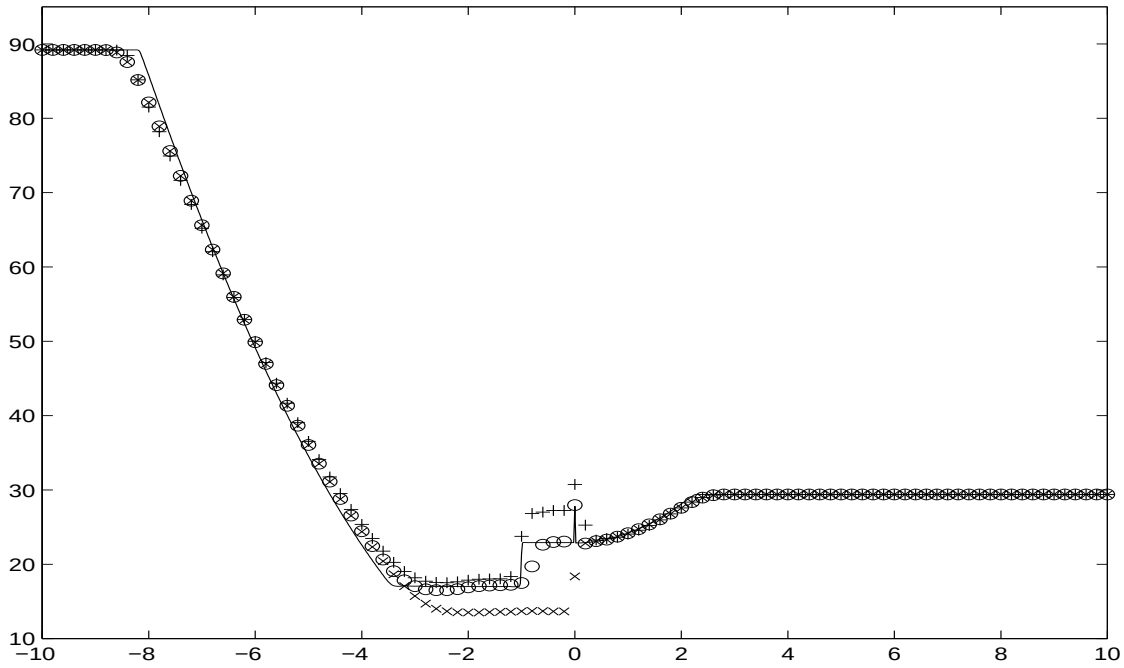

Figure 2.8 Example 2.2, the transonic case. Energy at t=0.5. Solid line: the exact solution; "o": the solution by the new method; "+": the solution of the interface method; "x": the solution of the cell average method.

3 The isothermal nozzle flow equations

Consider the system describing the evolution of an quasi-one-dimensional isothermal fluid in a nozzle

$$\partial_t(a\rho) + \partial_x(a\rho v) = 0, \tag{3.23}$$

$$\partial_t(a\rho v) + \partial_x(a\rho v^2 + ka\rho^\gamma) = p(\rho)\partial_x a, \tag{3.24}$$

$$\partial_t a = 0, \tag{3.25}$$

where ρ, v represent density and velocity of the fluid, $a(x) > 0$ is the cross-sectional area of the nozzle, $p(\rho)$ is the pressure given by the relation

$$p(\rho) = k\rho^\gamma.$$

The third equation (3.25) needs to be included as part of the system when the cross sectional area $a(x)$ contains discontinuities. When $a(x)$ is constant, equations (3.23)-(3.24) reduce to the standard isentropic equations.

The cell average method for above isothermal nozzle flow equations takes the form

$$\partial_t(a\rho)_j + \frac{(a\rho v)_{j+\frac{1}{2}} - (a\rho v)_{j-\frac{1}{2}}}{\Delta x} = 0 \tag{3.26}$$

$$\begin{aligned} & \partial_t (a\rho v)_j + \frac{(a\rho v^2 + ka\rho^\gamma)_{j+\frac{1}{2}} - (a\rho v^2 + ka\rho^\gamma)_{j-\frac{1}{2}}}{\Delta x} \\ = \quad & k{\rho_j}^\gamma \frac{a_{j+\frac{1}{2}} - a_{j-\frac{1}{2}}}{\Delta x} \end{aligned} \tag{3.27}$$

where the interface values can be obtained from a Riemann or approximate Riemann solver for the system (3.23)-(3.25) without source term.

When the steady state solution is smooth, the steady state solutions satisfy

$$a\rho v = C_1, \tag{3.28}$$

$$\frac{1}{2}v^2 + k\frac{\gamma}{\gamma-1}\rho^{\gamma-1} = C_2. \tag{3.29}$$

Furthermore, these steady state conditions also hold across a cross-sectional discontinuity [16].

In the same principle as the shallow water equations, our method for the isothermal nozzle flow equations can be described as follows. Assume a discontinuity of cross-section is contained in the cell $[x_1, x_2]$. Let a_i, ρ_i, v_i be the interface values of a, ρ, v at $x_i (i = 1, 2)$ respectively. Denote $H_i = a_i\rho_i v_i, G_i = \frac{1}{2}v_i^2 + k\frac{\gamma}{\gamma-1}{\rho_i}^{\gamma-1}, i = 1, 2$. Then we choose $\widehat{a}, H, G$ to be linear functions on $[x_1, x_2]$ so that $\widehat{a}(x_i) = a_i, H(x_i) = H_i, G(x_i) = G_i, i = 1, 2$. We choose $\widehat{\rho}, \widehat{v}$ from

$$\widehat{a}\widehat{\rho}\widehat{v} = H, \tag{3.30}$$

$$\frac{1}{2}\widehat{v}^2 + k\frac{\gamma}{\gamma-1}\widehat{\rho}^{\gamma-1} = G, \tag{3.31}$$

or $\widehat{\rho}$ from

$$\frac{1}{2}\frac{H^2}{\widehat{a}^2\widehat{\rho}^2} + k\frac{\gamma}{\gamma-1}\widehat{\rho}^{\gamma-1} = G \tag{3.32}$$

We then use the following expression

$$k\left(\frac{1}{\Delta x}\int_{x_1}^{x_2}\widehat{\rho}^\gamma dx\right)\frac{a_2 - a_1}{\Delta x}$$

to replace the source term approximation in cell average method (3.27). To obtain the integration value in the above expression, we use the same numerical strategy as for shallow water equations.

When the flow is subsonic or supersonic, there is no confusion to determine the right solution for $\widehat{\rho}$. In the transonic case, we also need a fix similar to that for the shallow water equations. This is illuminated by the fact that in the Riemann problem for isothermal nozzle flow equations, in the transonic case, the solution is in sonic state at the side of the cross sectional step which has a smaller area. For example, we assume the Mach number $|\frac{v_1}{\sqrt{k\gamma{\rho_1}^{\gamma-1}}}| > 1$, $|\frac{v_2}{\sqrt{k\gamma{\rho_2}^{\gamma-1}}}| < 1$, and $a_1 < a_2$. Let

$H_1 = a_1\rho_1 v_1$, ρ_3, v_3 satisfy $a_1\rho_3 v_3 = H_1$ and $|v_3| = \sqrt{k\gamma{\rho_3}^{\gamma-1}}$. Namely, we set $\rho_3 = (\frac{H_1^2}{k\gamma a_1^2})^{\frac{1}{\gamma+1}}$ and $v_3 = \frac{H_1}{a_1\rho_3}$. Let $G_1 = \frac{1}{2}v_3^2 + k\frac{\gamma}{\gamma-1}{\rho_3}^{\gamma-1}, H_2 = H_1, G_2 = G_1$. We then choose $\widehat{\rho}, \widehat{v}$ to satisfy (3.30)-(3.32). By choosing function $\widehat{\rho}$ to be solution of equation (3.32) corresponding to subsonic state because $|\frac{v_2}{\sqrt{k\gamma{\rho_2}^{\gamma-1}}}| < 1$ implies that the solution is in the subsonic state at the right side of the cross sectional step. We can similarly deal with other transonic case.

We now use two numerical examples to demonstrate that our method works well for calculating both unsteady and steady state solution for the isothermal nozzle flow equations.

The following two problems are Riemann problems studied in [16]. We choose $k = 1, \gamma = 4/3$. These two Reimann problems are solved numerically on the domain [-6, 6]. For spatial discretization, we use the Godunov flux for the homogeneous part of equations (3.23)-(3.24). The second order Runge-Kutta time discretization is used for time discretization. We take $\frac{\Delta t}{\Delta x} = 1/5$ for both problems. The zeorth extrapolation is used for numerical boundary conditions, and the "exact" solution is obtained using the new method with 1000 grid points.

Example 3.1. A Riemann problem with solution in the transonic state.

The initial data are $(\rho, v, a) = (4, -1.8, 1.5)$ when $x < 0$ and $(\rho, v, a) = (1, 2, 2.5)$ when $x > 0$. This is a transonic case. The solution reaches critical state at the left side of the cross-sectional jump and the energy $\frac{1}{2}v^2 + k\frac{\gamma}{\gamma-1}\rho^{\gamma-1}$ is a constant across the cross-sectional jump. For this problem, the cell average method immediately encounters the low density problem (which is impossible for the Roe scheme to handle [21]). The solution by the new method using 100 cells along with the "exact" solution are plotted in Figures 3.1-3.4. The solutions with the exact solution well. The numerical energy $\frac{1}{2}v^2 + k\frac{\gamma}{\gamma-1}\rho^{\gamma-1}$ is shown to be equal at two sides of cross-sectional jump, and captures the right-going shock on the right side of the cross-sectional jump. The interface method can also give very similar resolutions, but it does not keep the constant energy across the cross-sectional jump as well as the new method, and the gap does not decrease with increased space points, as shown by Figure 3.5 where the solutions of energy by the interface and cell average methods using 1000 cells are given. The figure is enlarged from the others to display the difference between the different methods.

Example 3.2. A Riemann problem with solution in both super- and sub-sonic states.

The initial data are $(\rho, v, a) = (4, -1.6, 1.5)$ when $x < 0$ and $(\rho, v, a) = (6, 1, 2.5)$ when $x > 0$. This is a mixed sub- and super-sonic case. The energy $\frac{1}{2}v^2 + k\frac{\gamma}{\gamma-1}\rho^{\gamma-1}$ at steady state is a constant across the cross-sectional jump. The solution from our method along with the "exact" solution in Figures 3.6-3.8. These solutions match well with the exact solution. On the other hand, solutions by the interface method

and the cell average method do not preserve the constant energy across the cross-sectional jump with a high accuracy. Figure 3.9 depicts the energy by the interface method and the cell average method using 1000 cells. This figure is enlarged near the bottom step. The interface method behaves better than cell average method, but both methods have gaps across the cross-sectional jump whicj do not decrease when more grid points are used. We plot the steady state solutions by our new method using 100 cells in Figure 3.10. One can see that the steady state energy is a very good approximation of a constant, as the exact solution should be.

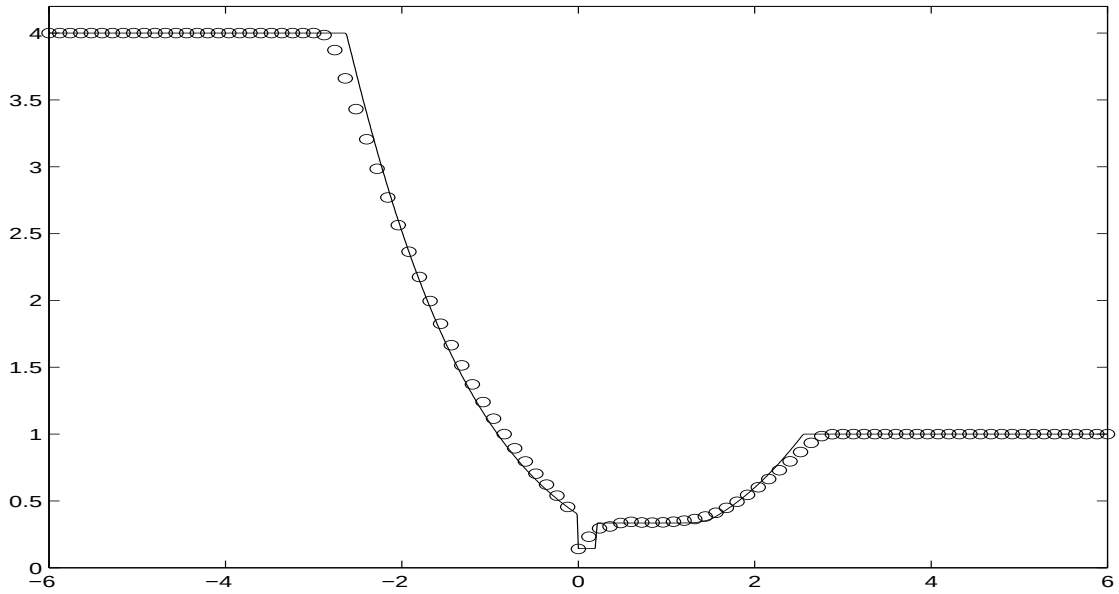

Figure 3.1 Example 3.1, the transonic case. Density at t=0.8. Solid line: the exact solution; "o": the solution by the new method using 100 cells.

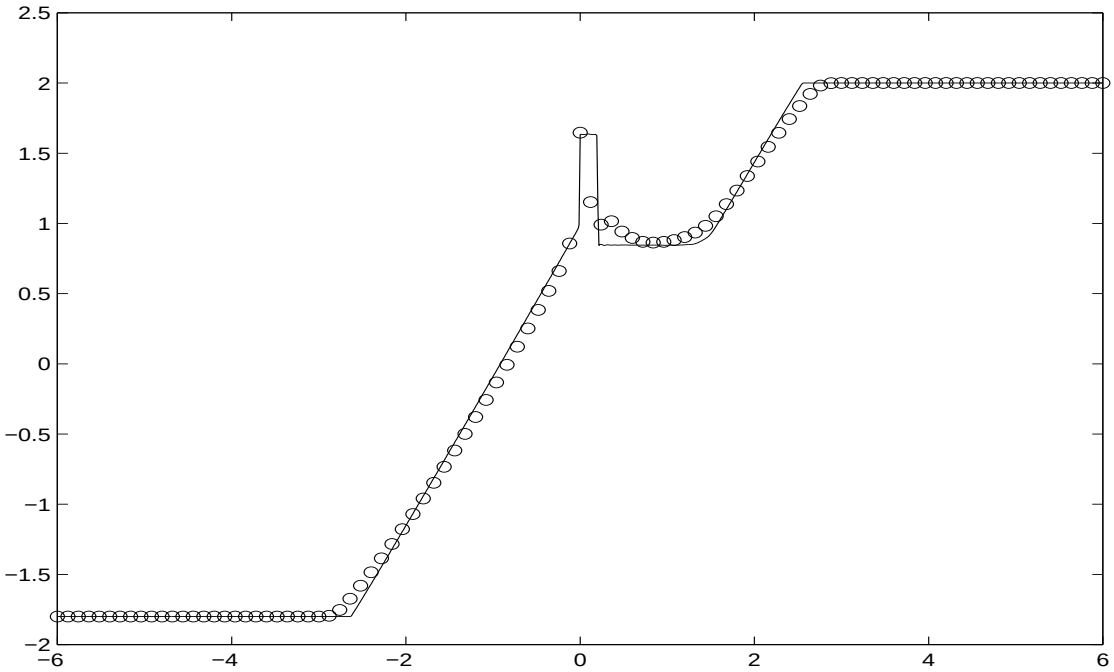

Figure 3.2 Example 3.1, the transonic case. Velocity at t=0.8. Solid line: the exact solution; "o": the solution by the new method using 100 cells.

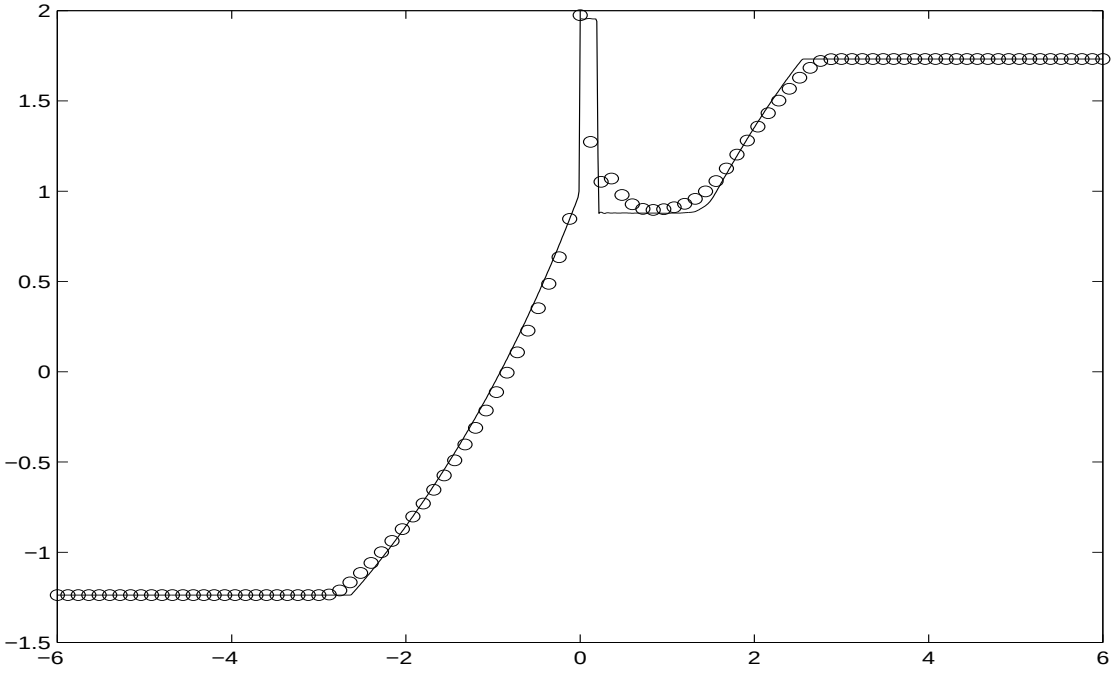

Figure 3.3 Example 3.1, the transonic case. Mach number at t=0.8. Solid line: the exact solution; "o": the solution by the new method using 100 cells.

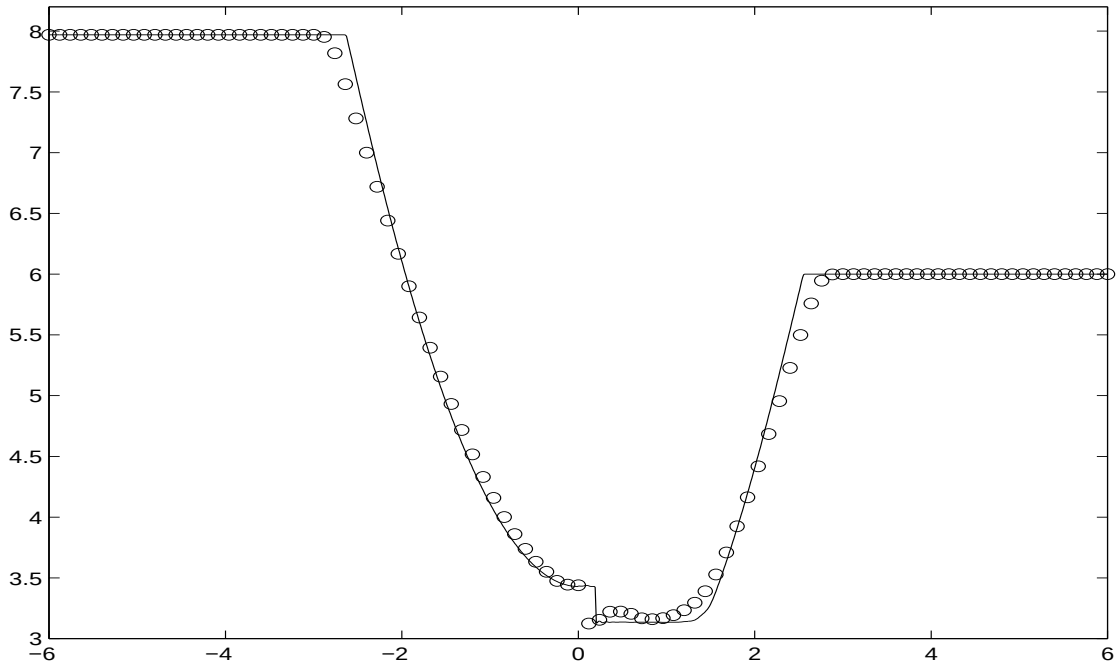

Figure 3.4 Example 3.1, the transonic case. Energy at t=0.8. Solid line: the exact solution; "o": the solution by the new method using 100 cells.

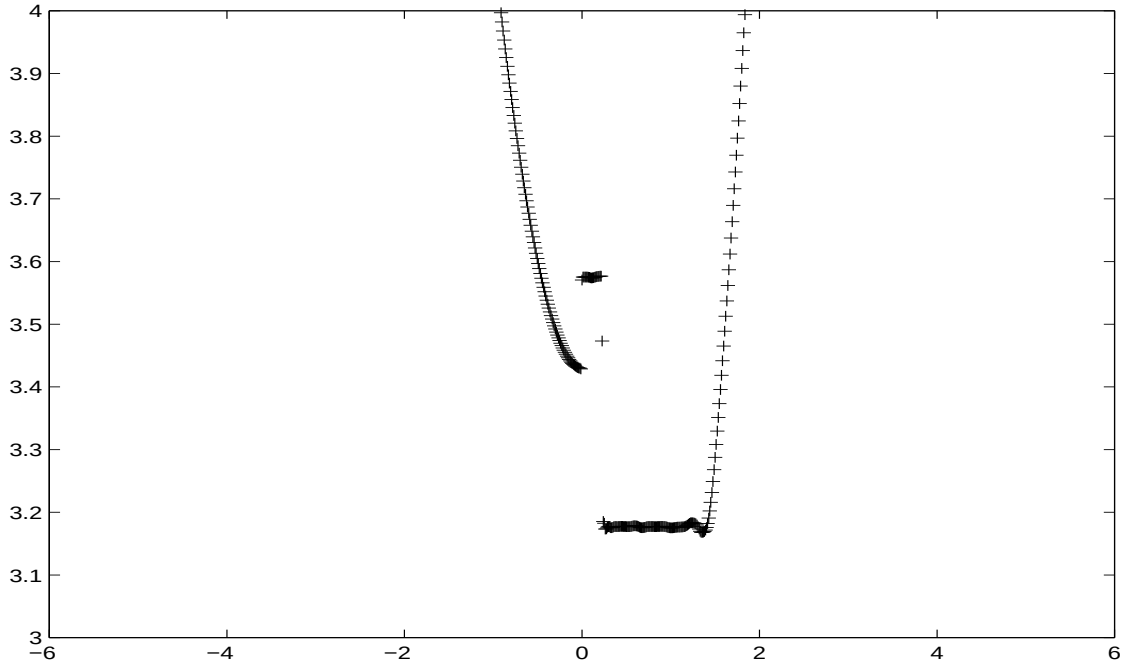

Figure 3.5 Example 3.1, the transonic case. A close looks of the energy at $t = 0.8$ by the interface method using 1000 cells.

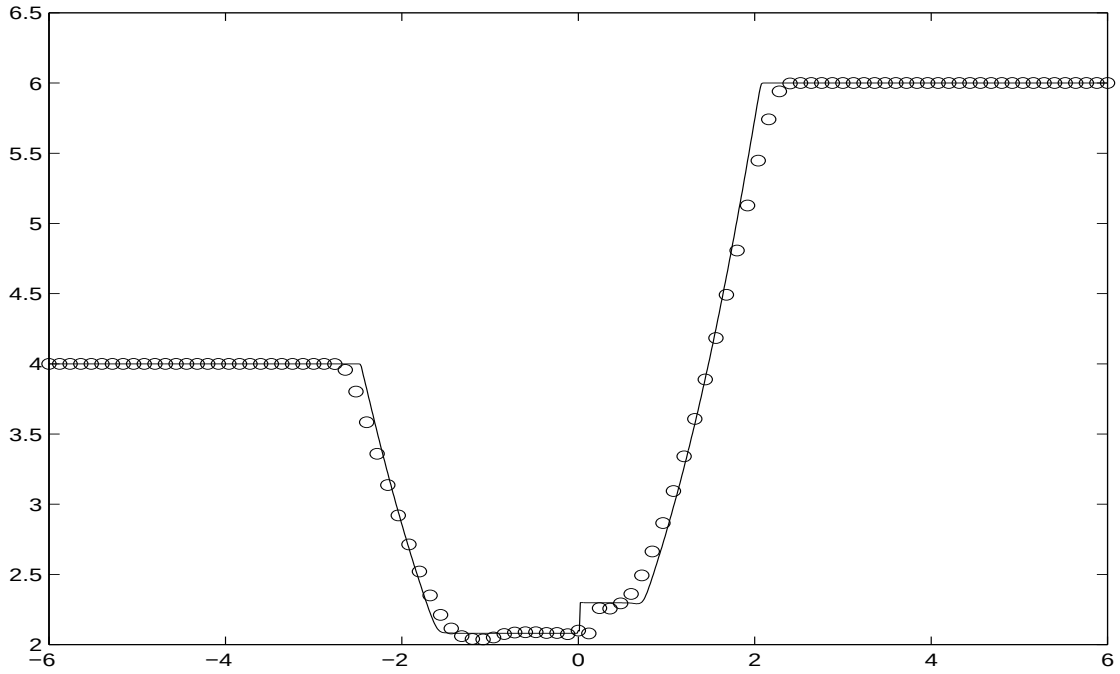

Figure 3.6 Example 3.2, mixed sub- and super-sonic case. Density at t=0.8. Solid line: the exact solution; "o": the solution by the new method using 100 cells.

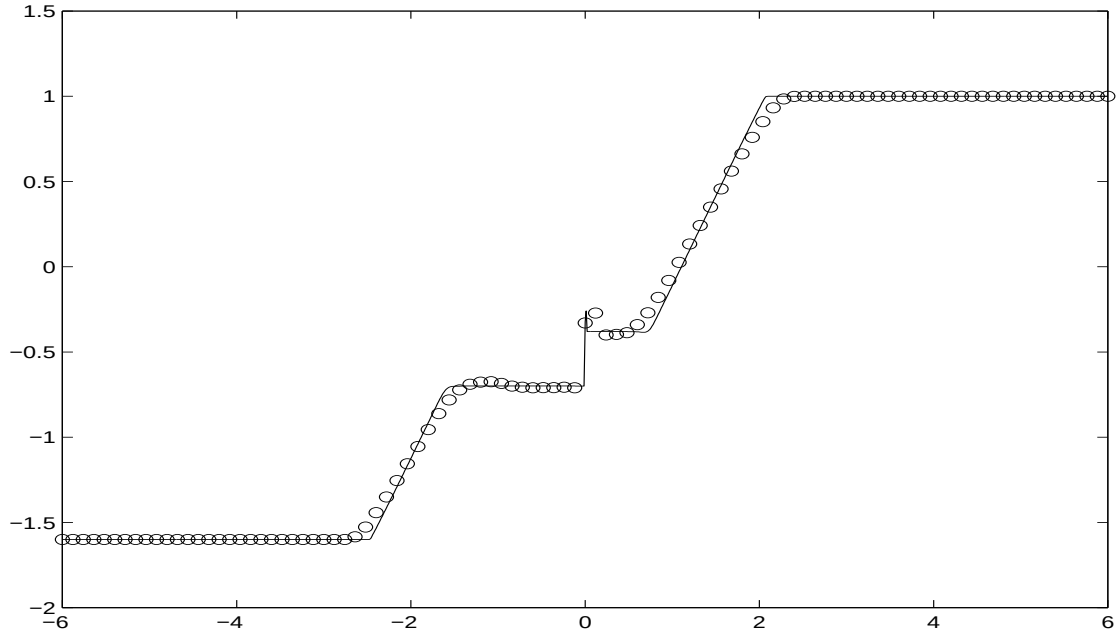

Figure 3.7 Example 3.2, mixed sub- and super-sonic case. Velocity at $t = 0.8$. Solid line: the exact solution; "o": the solution by the new method using 100 cells.

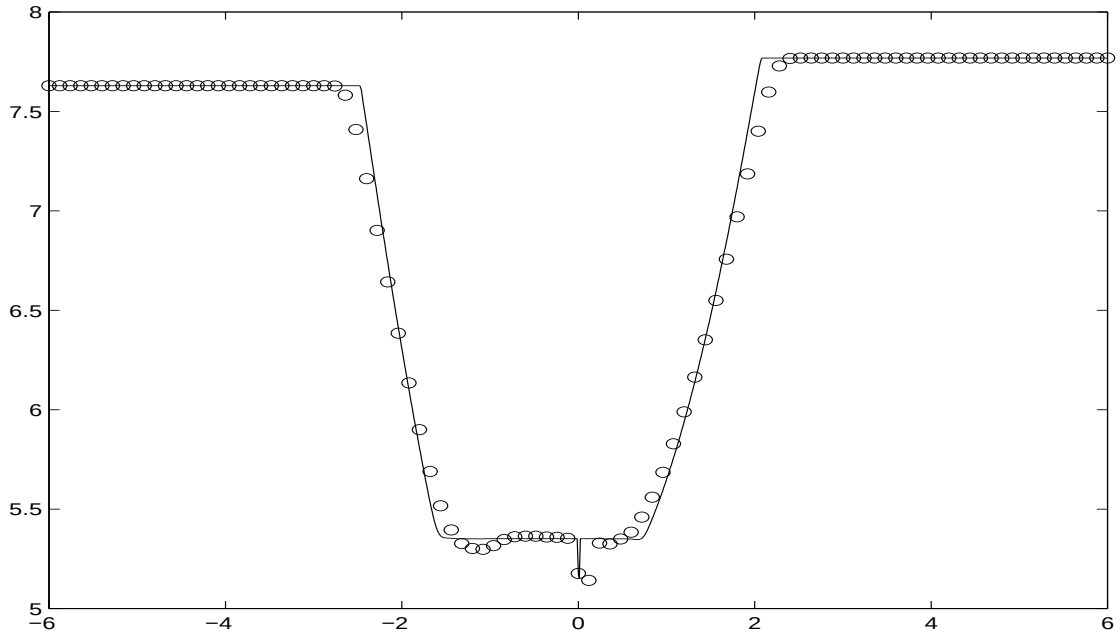

Figure 3.8 Example 3.2, mixed sub- and super-sonic case. Energy at $t = 0.8$. Solid line: the exact solution; "o": the solution by the new method using 100 cells.

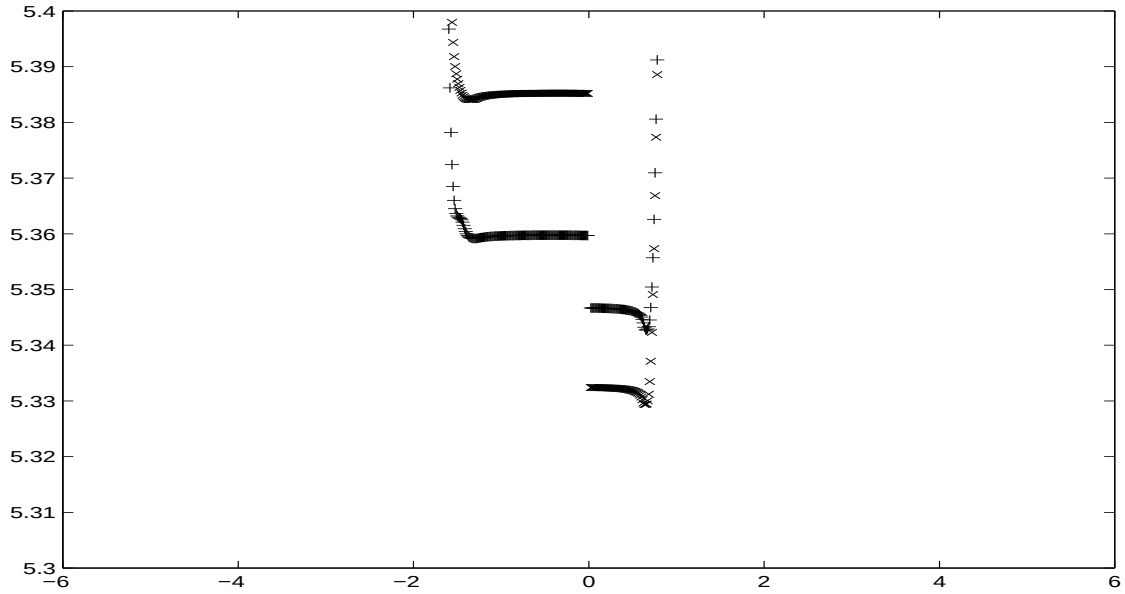

Figure 3.9 Example 3.2, mixed sub- and super-sonic case. A close look of the energy. "+": the solution of the interface method using 1000 cells; "x": the solution of the cell average method using 1000 cells.

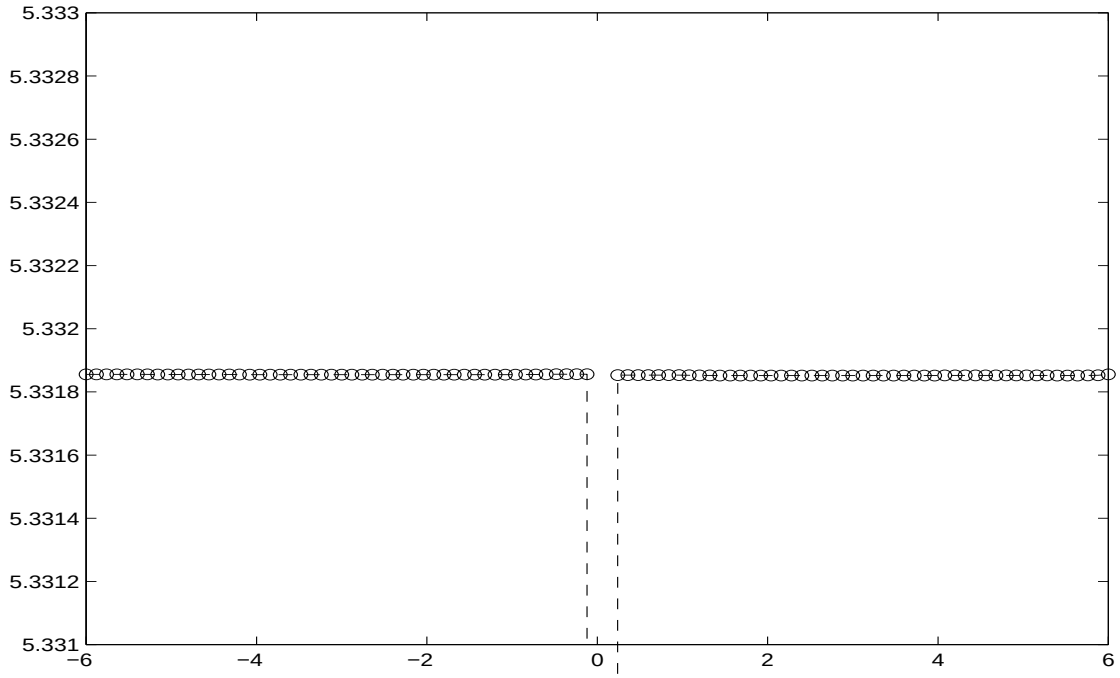

Figure 3.10 Example 3.2, mixed sub- and super-sonic case. Energy at steady state by our new method using 100 cells.

4 The non-isothermal nozzle flow equations

The one-dimensional non-isothermal nozzle flow equations can be described by the following Euler equations with a geometric source term

$$\partial_t(a\rho) + \partial_x(a\rho v) = 0, \tag{4.33}$$
$$\partial_t(a\rho v) + \partial_x(a\rho v^2 + Pa) = P\partial_x a, \tag{4.34}$$
$$\partial_t(aE) + \partial_x(v(E+P)a) = 0; \tag{4.35}$$

where ρ, v, P, E are respectively density, velocity, pressure, and total energy, $a(x) > 0$ is area of the nozzle. For a polytropic gas, the equation of state is given by

$$P = (\gamma - 1)(E - \frac{1}{2}\rho v^2). \tag{4.36}$$

The cell average method for above non-isothermal nozzle flow equations takes the form

$$\partial_t(a\rho)_j + \frac{(a\rho v)_{j+\frac{1}{2}} - (a\rho v)_{j-\frac{1}{2}}}{\Delta x} = 0, \tag{4.37}$$
$$\partial_t(a\rho v)_j + \frac{(a\rho v^2 + Pa)_{j+\frac{1}{2}} - (a\rho v^2 + Pa)_{j-\frac{1}{2}}}{\Delta x}$$

$$= P_j \frac{a_{j+\frac{1}{2}} - a_{j-\frac{1}{2}}}{\Delta x}, \tag{4.38}$$

$$\partial_t (aE)_j + \frac{(v(E+P)a)_{j+\frac{1}{2}} - (v(E+P)a)_{j-\frac{1}{2}}}{\Delta x} = 0; \tag{4.39}$$

where $a_{j+\frac{1}{2}} = a(x_{j+\frac{1}{2}})$. The interface values are produced by the Roe method for the non-isothermal nozzle flow equations (4.33)-(4.35) without the source term, namely the Euler equations.

The steady state solution satisfies

$$a\rho v = C_1, \tag{4.40}$$

$$av(\gamma E - \frac{\gamma - 1}{2}\rho v^2) = C_2, \tag{4.41}$$

$$\frac{\rho^\gamma}{E - \frac{1}{2}\rho v^2} = C_3. \tag{4.42}$$

Assume a discontinuity of the cross-section is contained in the cell $[x_1, x_2]$. Let a_i, ρ_i, v_i, E_i be the interface values of a, ρ, v, E at $x_i, i = 1, 2$ respectively. Denote $H_i = a_i\rho_i v_i, G_i = a_i v_i(\gamma E_1 - \frac{\gamma - 1}{2}\rho_i v_i^2), F_i = \frac{{\rho_i}^\gamma}{E_i - \frac{1}{2}\rho_i v_i^2}, i = 1, 2$. Then we choose $\widehat{a}, H, G, F$ to be linear functions on $[x_1, x_2]$ so that $\widehat{a}(x_i) = a_i, H(x_i) = H_i, G(x_i) = G_i, F(x_i) = F_i, i = 1, 2$. We choose $\widehat{\rho}, \widehat{v}, \widehat{E}$ satisfying

$$\widehat{a}\widehat{\rho}\widehat{v} = H, \tag{4.43}$$

$$\widehat{a}\widehat{v}(\gamma\widehat{E} - \frac{\gamma - 1}{2}\widehat{\rho}\widehat{v}^2) = G, \tag{4.44}$$

$$\frac{\widehat{\rho}^\gamma}{\widehat{E} - \frac{1}{2}\widehat{\rho}\widehat{v}^2} = F. \tag{4.45}$$

Define $\widehat{P}$ by

$$\widehat{P} = (\gamma - 1)(\widehat{E} - \frac{1}{2}\widehat{\rho}\widehat{v}^2),$$

We then use the following expression

$$\left(\frac{1}{\Delta x}\int_{x_1}^{x_2} \widehat{P} dx\right) \frac{a_2 - a_1}{\Delta x}.$$

to replace the source term approximation in the cell average method (4.38). The numerical integration strategy is similar as before mentioned.

When the flow is transonic over the cross-sectional discontinuity, we also need the fix to choose the solutions from (4.43)-(4.45). This is essentially the same as the isothermal nozzle flow equations.

We now give a numerical example to show the performance of our method for calculating both unsteady and steady state solution for the non-isothermal nozzle flow equations.

Example 4.1. The problem to be tested contains a transonic shock at steady state. This is a problem modified from a continuous bottom problem. Consider a divergent nozzle from [7] with

$$a(x) = 1.398 + 0.347 \tanh(0.8x - 4),$$

as shown in Figure 4.1. The computational domain is $0 \leq x \leq 10$. The left boundary conditions are $(\rho_l, v_l, E_l) = (0.502, 1.897, 1.299)$, the right boundary conditions are $\rho_r = 0.776$. We choose the initial values as $(\rho, v, E) = (0.502, 1.8974, 1.299)$ when $x < 5$ and $(\rho, v, E) = (0.776, 0.506, 1.979)$ when $x > 5$. We take $\frac{\Delta t}{\Delta x} = 1/4$, and use the Roe flux for the convection and a second order Runge-Kutta time discretization. The density in the steady state solutions from cell average method using 100 cells are plotted in Figure 4.2. The steady state solution contains a standing transonic shock.

We slightly modify this continuous cross-section to be a discontinuous one

$$a(x) = \begin{cases} 1.05, & 0 \leq x \leq 2, \\ 1.4452 + 0.3 \tanh(0.8x - 4), & 2 < x \leq 10. \end{cases}$$

Figure 4.3 plots the shape of the nozzle with this cross-sectional area.

Still using the same initial values and boundary conditions, the density and $\frac{\rho^\gamma}{P}$ at t=0.5 from our method using 100 cells, and using 4000 cells–which serve as the "exact" solution, are plotted in Figures 4.4-4.5 respectively. One may notice that the quantity $\frac{\rho^\gamma}{P}$ already reaches the same constant at two sides of the cross-sectional discontinuity at t=0.5.

Figures 4.6-4.7 plot respectively the density and the quantity $\frac{\rho^\gamma}{P}$ in the steady state by our new method using 100 cells. The steady state solution of $\frac{\rho^\gamma}{P}$ reaches the same constant at two sides of the cross-sectional discontinuity.

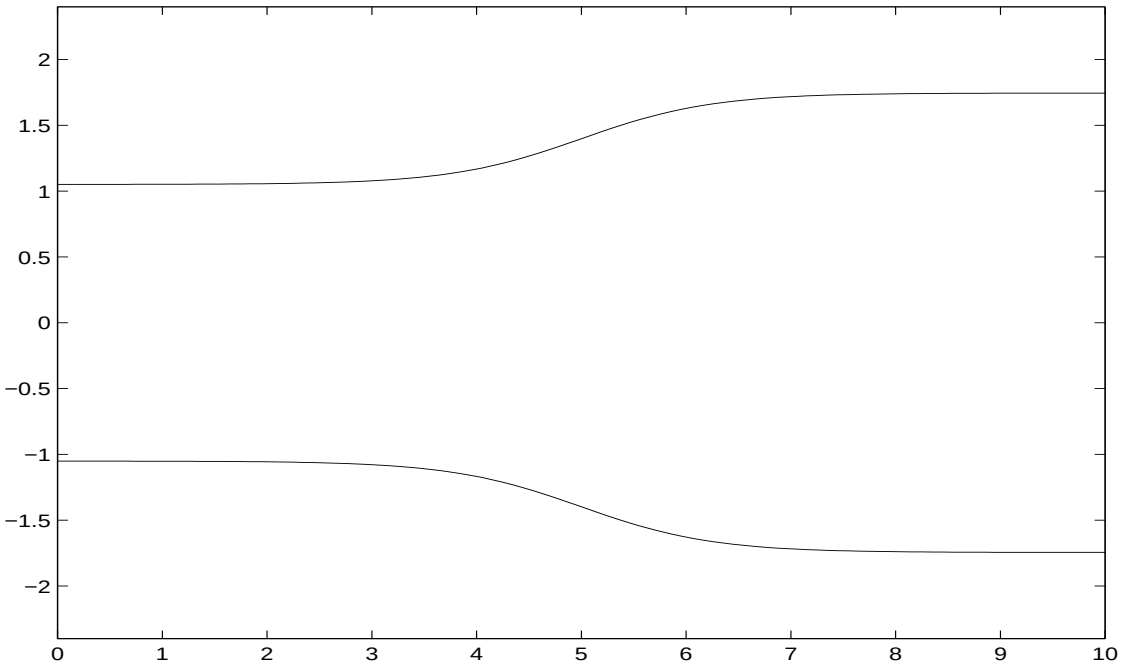

Figure 4.1 Example 4.1, the divergent nozzle.

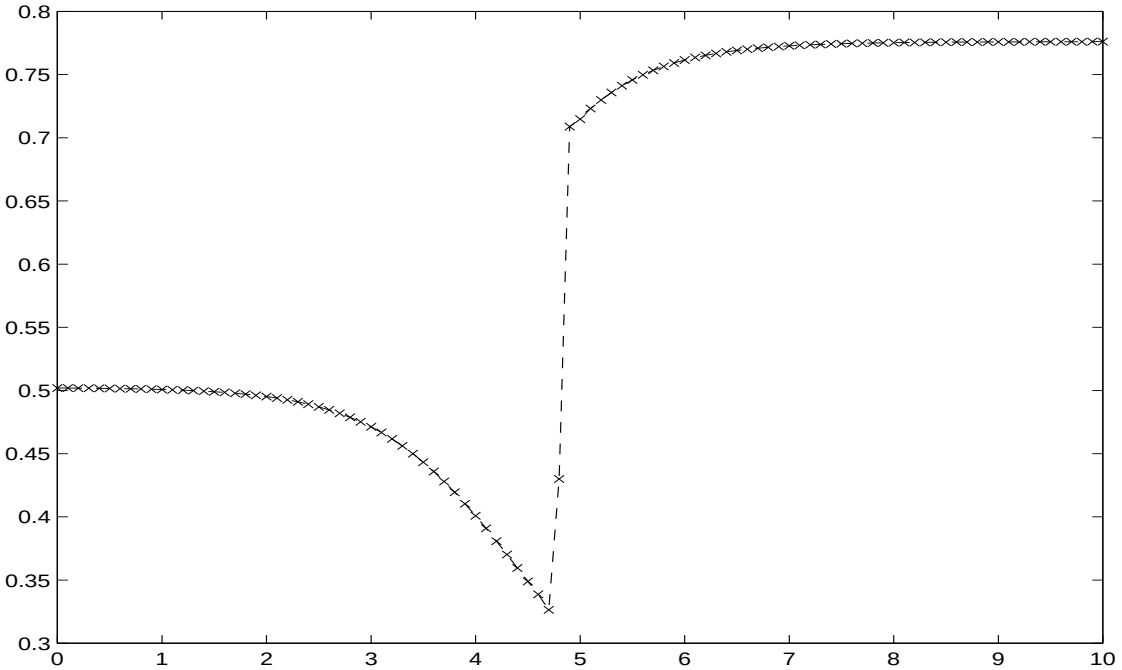

Figure 4.2 Example 4.1, steady state density by the cell average method using 100 cells.

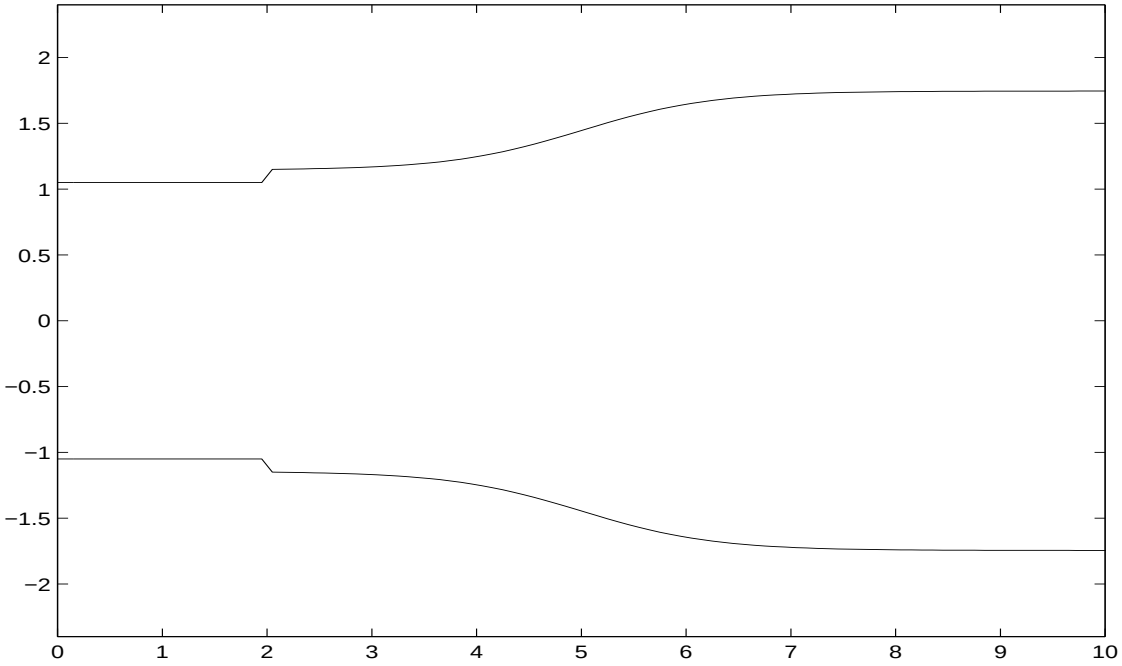

Figure 4.3 Example 4.1, a nozzle with discontinuous cross-sectional area.

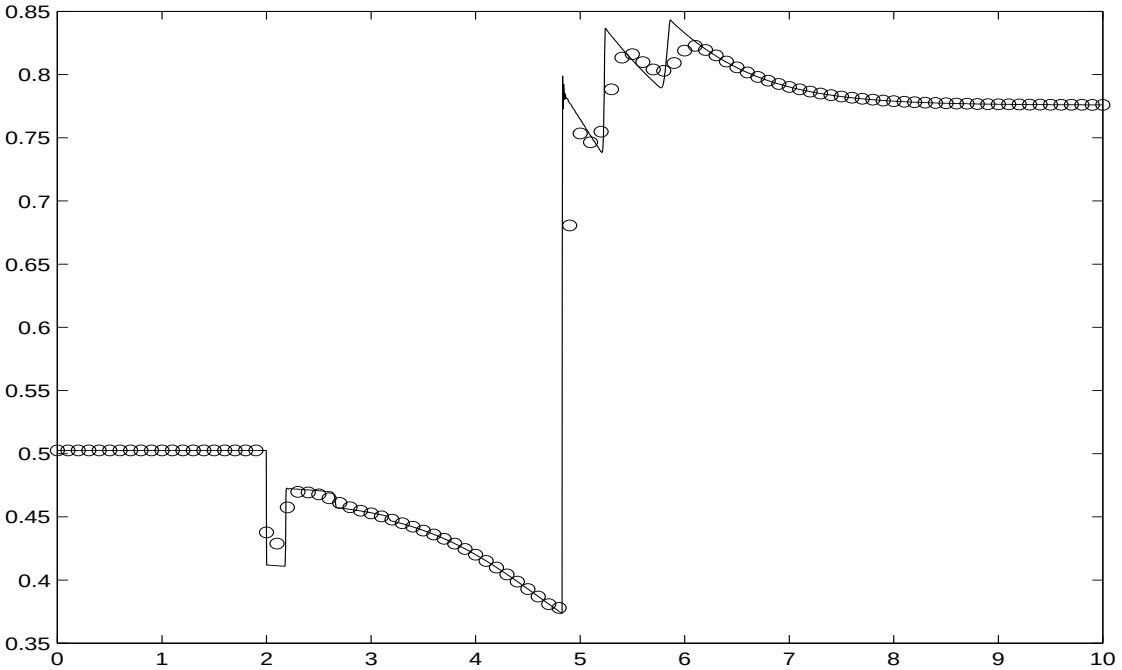

Figure 4.4 Example 4.1, density at t=0.5. Solid line: the exact solution; "o": the solution by the new method using 100 cells.

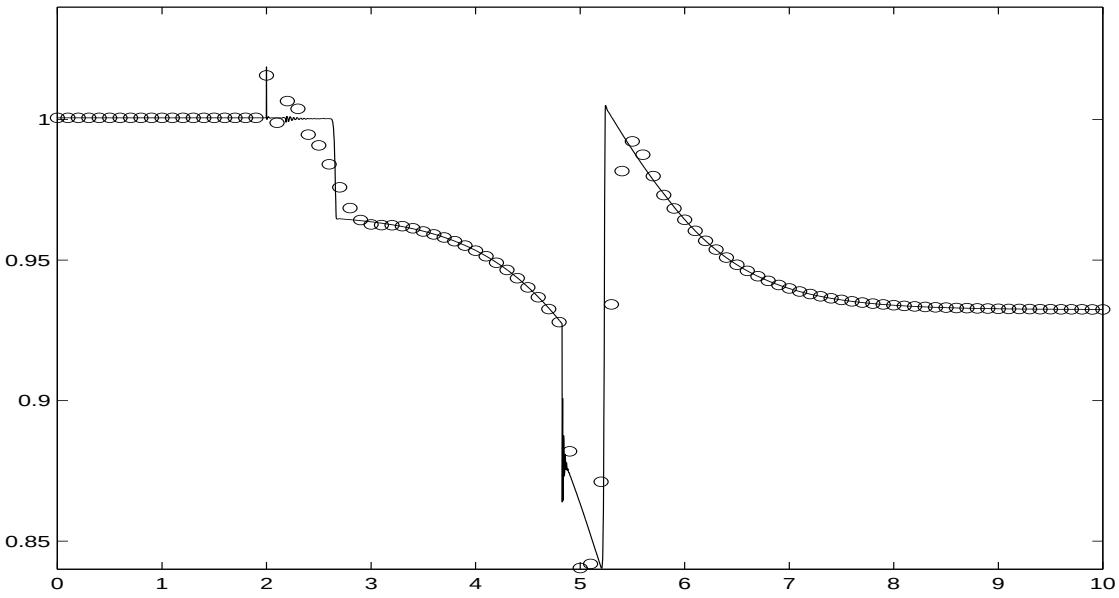

Figure 4.5 Example 4.1, Solutions of $\frac{\rho^\gamma}{P}$ at t=0.5. Solid line: the exact solution; "o": the solution by our new method using 100 cells.

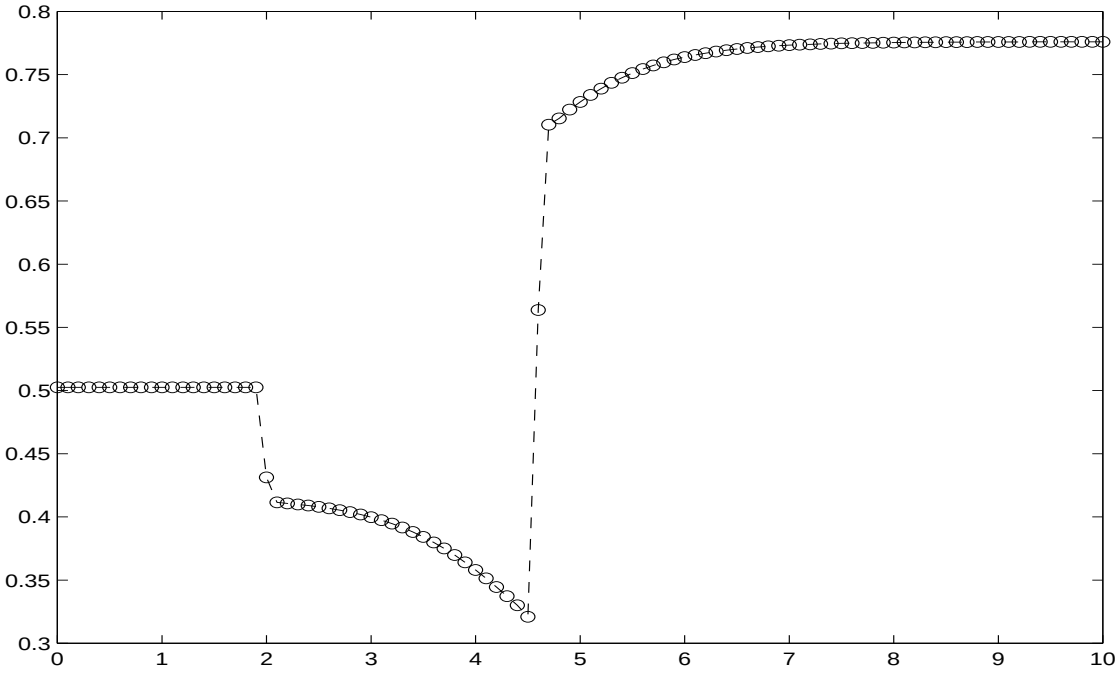

Figure 4.6 Example 4.1, steady state density by our new method using 100 cells.

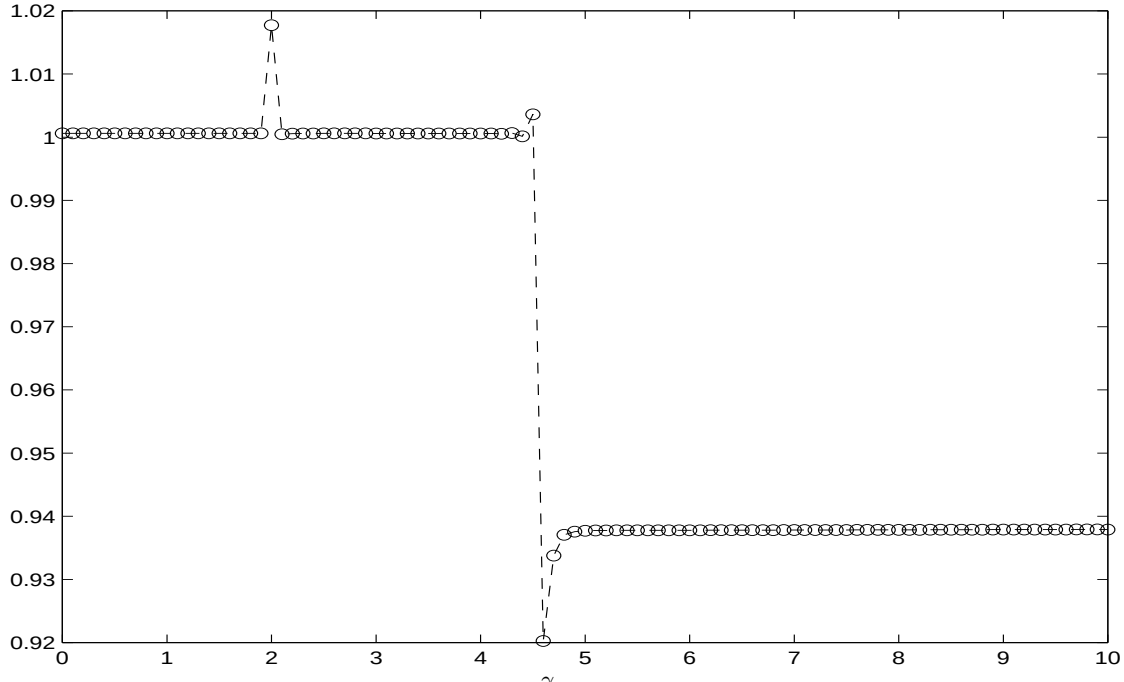

Figure 4.7 Example 4.1, solutions of $\frac{\rho^\gamma}{P}$ at steady state by our new method using 100 cells.

References

[1] F. Alcrudo and F. Benkhaldoun, Exact solutions to the Riemann problem of the shallow water equations with a bottom step, Computers Fluids 30, 643-671 (2001).

[2] E. Audusse, F. Bouchut, M.-O. Bristeau, R. Klein and B. Perthame, A fast and stable well-balanced scheme with hydrostatic reconstruction for shallow water flows, SIAM J. Sci. Comp., to appear.

[3] A. Bernudez and M.E. Vazquez, Upwind methods for hyperbolic conservation laws with source terms, Computers Fluids 23, 1049-1071 (1994).

[4] R. Botchorishvili, B. Perthame and A. Vasseur, Equilibrium schemes for scalar conservation laws with stiff sources, Math. Comp. 72(241), 131-157 (2003).

[5] A. Chinnayya and A.Y. Le Roux, A new general Riemann solver for the shallow-water equations with friction and topography, preprint 1999.

[6] T. Gallouët, J.-M. Hérard and N. Seguin, Some approximate Godunov schemes to compute shallow-water equations with topography, Computers Fluids 32, 479-513 (2003).

[7] H.M. Glaz and T.P. Liu, The asymptotic analysis of wave interactions and numerical calculations of transonic nozzle flow, Adv. in Appl. Math. 5, 111-146 (1984).

[8] S.K. Godunov, Finite difference schemes for numerical computation of solutions of the equations of fluid dynamics, Math. USSR Sbornik 47, 271-306 (1959).

[9] L. Gosse, A well-balanced flux-vector splitting scheme designed for hyperbolic systems of conservation laws with source terms, Comp. Math. Appl. 39, 135-159 (2000).

[10] L. Gosse, A well-balanced scheme using non-conservative products designed for hyperbolic systems of conservation laws with source terms, Math. Models Methods Appl. Sci. 11(2), 339-365 (2001).

[11] L. Gosse and A.-Y. Le Roux, A well-balanced scheme designed for inhomogeneous scalar conservation laws, C.R. Acad. Sc., Paris. Sér I 323, 543-546 (1996).

[12] J.M. Greenberg and A.-Y. Le Roux, A well-balanced scheme for the numerical processing of source terms in hyperbolic equations, SIAM J. Num. Anal. 33, 1-16 (1996).

[13] J.M. Greenberg, A.-Y. Le Roux, R. Baraille and A. Noussair, Analysis and approximation of conservation laws with source terms, SIAM J. Num. Anal. 34, 1980-2007 (1997).

[14] S. Jin, A steady-state capturing method for hyperbolic system with geometrical source terms, Math. Model. Num. Anal. 35, 631-646 (2001).

[15] A. Kurganov and D. Levy, Central-upwind schemes for the Saint-Venant system, Math. Model. Numer. Anal. 36(3), 397–425 (2002).

[16] P.G. LeFloch and M.D. Thanh, The riemann problem for fluid flows in a nozzle with discontinuous cross-section, Comm. Math. Sci. 1, 763-797 (2003).

[17] R.J. LeVeque, Numerical Methods for Conservation Laws, Birkhauser-Verlag, Basel, 1990.

[18] R.J. LeVeque, Balancing source terms and flux gradients in high-resolution Godunov methods: the quasi-steady wave-propagation algorithm, J. Comp. Phys. 146, 346-365 (1998).

[19] B. Perthame, C. Simeoni, A kinetic scheme for the Saint-Venant system with a source term, CALCOLO 38(4), 201-231 (2001).

[20] Ch. Makridakis and Th. Katsaounis, Relaxation models and finite element schemes for the shallow water equations, in Hyperbolic Problems: Theory, Numerics, Applications, Proceedings of the Ninth International Conference on Hyperbolic Problems held in CalTech, Pasadena, March 25-29, 2002 Hou, Thomas Y.; Tadmor, Eitan (Eds.)

[21] J.J. Quick, Int. J. Num. Methods Fluids 18, 555 (1994).

[22] P.L. Roe, Approximate Riemann solvers, parameter vectors, and difference schemes, J. Comp. Phys. 43, 357-372 (1981).

[23] P.L. Roe, Upwinding differenced schemes for hyperbolic conservation laws with source terms, in Nonlinear Hyperbolic Problems, Proc. Adv. Res. Workshop, St. Étienne, 1986, Lect. Notes Math., Springer, Berline, 1270, 41-45 (1987).

[24] M.E. Vazquez-Cendon, Improved treatment of source terms in upwind schemes for shallow water equations in channels with irregular geometry, J. Comp. Phys. 148, 497-526 (1999).

[25] K. Xu, A well-balanced gas-kinetic scheme for the shallow water equations with source terms, J. Comp. Phys. 178(2), 533-562 (2002).